



## Electrodeposition and characterization of Fe<sub>80</sub>Ga<sub>20</sub> alloy films

D. Iselt<sup>a,b,\*</sup>, U. Gaitzsch<sup>a</sup>, S. Oswald<sup>a</sup>, S. Fähler<sup>a</sup>, L. Schultz<sup>a,b</sup>, H. Schlörb<sup>a</sup>

<sup>a</sup> IFW Dresden, Leibniz Institute for Solid State and Materials Research Dresden, PF 27 01 16, 01171 Dresden, Germany

<sup>b</sup> TU Dresden, Faculty of Mechanical Engineering, 01062 Dresden, Germany

### ARTICLE INFO

#### Article history:

Received 6 December 2010

Received in revised form 8 February 2011

Accepted 11 March 2011

Available online 22 March 2011

#### Keywords:

Galfenol

Fe<sub>100-x</sub>Ga<sub>x</sub>

Thin film

Electrodeposition

Magnetostriction

### ABSTRACT

Due to its high magnetostriction and good mechanical properties Fe<sub>80</sub>Ga<sub>20</sub> is interesting for magnetostrictive microactuators and sensors. Here we use electrodeposition to grow Fe–Ga films onto Au and Pt coated Si substrates by potentiostatic and pulse potential deposition. Composition, microstructure and structure are analysed. The desired composition of Fe<sub>80</sub>Ga<sub>20</sub> was obtained at  $-1.4 V_{SCE}$  and  $-1.5 V_{SCE}$ , respectively. The origin of low reproducibility and high oxygen content up to 50 at.% is investigated. Optimum deposition conditions to achieve dense, homogeneous films with low oxygen content are identified. In these films the saturation magnetization reaches a maximum value of 1.7 T confirming the high quality of electrodeposited films.

© 2011 Elsevier Ltd. All rights reserved.

### 1. Introduction

Magnetostrictive materials change their dimensions with changes in magnetization and are therefore interesting for actuator and sensor applications. Since the discovery of magnetostriction of iron by James Joule in 1842, intensive research work has been undertaken to understand the effect [1–5], to increase the length changes by addition of non-magnetic elements (like Al or rare earth elements) [2,6–8] and, recently, to use these materials as actuation and sensing devices [9–13]. However, any application requires besides a high magnetostrictive constant, also good mechanical properties. Common ferromagnetic metals show good mechanical properties, such as ductility, but the magnetostrictive strain is rather low (several  $10 \times 10^{-6}$  up to  $100 \times 10^{-6}$ ) [7,14]. Rare earth alloys show a “giant” magnetostrictive strain in the order of  $1000 \times 10^{-6}$  (Terfenol-D, Tb<sub>0.3</sub>Dy<sub>0.7</sub>Fe<sub>2</sub>) [5] but they are brittle. A promising candidate to overcome the mechanical limitations of rare earth alloys is Galfenol, an alloy of iron and gallium, which combines mechanical strength (Fe<sub>83</sub>Ga<sub>17</sub> endures tensile stresses up to 440 MPa with strains approaching 0.25% before failure) [15] with “large” magnetostrictive strains (up to 400 ppm for quenched Fe<sub>80</sub>Ga<sub>20</sub> single crystals) [8]. Further advantages are  $H(\text{sat}) < 1 \text{ kOe}$ , low temperature dependence in the range from  $-20$  to  $80^\circ\text{C}$  [16,17] and comparatively high oxidation stability. Most of the work on this material has been done on bulk single crystals, polycrystals and

rods. Focusing on smaller dimensions a few groups investigated the deposition of thin films by physical methods. Butera et al. [18] deposited 900 nm thin films on (1 0 0)MgO substrates using sputter deposition, and were able to find the correlation between sputter pressure and growth behaviour. A linear dependence of the FeGa lattice parameter was found by Dunlap et al. [19] in 2006: with increasing Ga content the lattice parameter increases. Wang [20] analysed the influence of the sputter gas, thermal treatment and deposition under external magnetic field. Using a sputter pressure of 1.2 Pa under argon atmosphere he obtained a saturation magnetostriction  $\lambda_S$  of up to 50 ppm. By depositing in a magnetic field the sample texture changes from (1 1 0) to (1 0 0) orientation. Additional heat pre-treatment has further improved the soft magnetic properties. The influence of the partial pressure of the sputtering gas on magnetic properties of Fe<sub>100-x</sub>Ga<sub>x</sub> ( $19 \leq x \leq 23$ ) has been investigated by Javed et al. [4]. Here, the best soft magnetic properties for sensor applications are obtained when growing at low sputter pressures of 3  $\mu\text{bar}$ . Adolphi et al. [21] investigated the influence of film thickness and seed layers on the film texture and consequences of texture on the magnetic properties. They obtained a high spontaneous polarization of  $J_S = 1.45 \text{ T}$  in 1.3  $\mu\text{m}$  thick films and summarised that the value of magnetostrictive parameters and the relative permeability are promising for sensor bending applications.

Compared to physical methods, electrochemical deposition provides an easy and low cost method to produce thin films over large areas, in complex geometries and does not require high vacuum conditions. However, the electrodeposition of FeGa had been rarely investigated, since it is hard to deposit Ga [22–24] and its alloys [25] from aqueous electrolytes. The main reasons for this are the

\* Corresponding author at: IFW Dresden, Helmholtzstrasse 20, D-01069 Dresden, Germany. Tel.: +49 351 4659 290; fax: +49 351 4659 500.

E-mail address: [d.iselt@ifw-dresden.de](mailto:d.iselt@ifw-dresden.de) (D. Iselt).

highly negative standard potential of  $\text{Ga}^{3+}/\text{Ga}$  ( $E^{00} = -0.560\text{ V}$ ) [23] and its strong tendency to hydrolyse [24]. McGary reported first on the electrochemical deposition of Fe–Ga alloys, the fabrication of nanoscale Galfenol structures [26] and their use as sensor systems for sonar applications [10]. Using a Watt's type electrolyte containing iron(II) and gallium(III) sulphates, boric acid and ascorbic acid Fe–Ga nanowire arrays have been deposited into anodic aluminium oxide templates at a constant potential of  $-1.36\text{ V}$ . The Ga content was found to decrease along the length of the wires and the nanowire arrays were magnetically soft and slightly anisotropic [26]. However, even for films no crystalline Fe–Ga phase was observed [10] and no statement was made about the oxygen content of the deposit. Another group investigated the electrochemical fabrication of magnetic multilayered films and nanowire arrays containing Fe–Ga in order to achieve novel magnetostrictive behaviour [27,28]. By adjusting both, the electrolyte composition and deposition potential,  $\text{Fe}_{78}\text{Ga}_{22}$  films with a crystalline (Fe, Ga) solid-solution phase were obtained. Multilayered nanowire arrays were deposited from a single electrolyte by applying different constant potentials. A novel magnetostrictive behaviour was explained by the formation of twisted spin structures. Very recently, a detailed study of Fe–Ga codeposition was published by McGary [29]. Using a Hull cell, where the deposition current density varies across the cathode, metallic iron, Galfenol, oxide and Ga-rich metal films have been produced. Complexing the Ga ions with citrate and varying the ratio of  $\text{Ga}^{3+}/\text{Fe}^{2+}$  ions and the current density allowed to control the composition as well as grain size and texture of the alloy.

Our present study aims on the preparation and detailed characterization of Fe–Ga alloy films with a gallium concentration of around 20 at.%. The particular focus is to investigate the origin of the high oxygen content and to identify appropriate deposition parameters for homogeneous, dense alloy films with low oxygen content that are promising to achieve a high magnetostriction constant.

## 2. Experimental details

Oxidized (1 0 0)Si wafers were coated with either Au or Pt which acts as working electrodes for the deposition experiments. Based on McGary's work [10] the electrolyte consists of an aqueous solution of  $0.3\text{ M FeSO}_4 \cdot 7\text{H}_2\text{O}$ ,  $0.06\text{ M Ga}_2(\text{SO}_4)_3 \cdot 18\text{H}_2\text{O}$ ,  $0.5\text{ M}$  boric acid ( $\text{H}_3\text{BO}_3$ ) as a buffer and  $0.04\text{ M}$  ascorbic acid ( $\text{C}_6\text{H}_8\text{O}_6$ ) as an antioxidant agent, where the pH was adjusted to 1.5 by adding sulphuric acid. For each experiment 20 ml of fresh electrolyte was used. All deposition experiments were performed at room temperature in a three electrode arrangement placed in a Teflon cell. A Pt sheet was used as the counter electrode and a Saturated Calomel Electrode (SCE) as reference electrode. The electrode potentials all refer to the potential of the SCE ( $-241\text{ mV}_{\text{SHE}}$ ). Deposition experiments were carried out using an EG&G Potentiostat/Galvanostat Model 263A.

Sample surface and cross sectional morphologies as well as film thickness were examined using high-resolution scanning electron microscopy (HR-SEM Leo 1530 Gemini, Zeiss) and focused ion beam technique (FIB, Zeiss Cross Beam 1540XB), respectively. The integral composition was obtained by energy dispersive X-ray spectroscopy (EDX, Leo 1530 Gemini, Zeiss with Si(Li)-detector). To estimate the oxygen content and the detailed oxygen binding behaviour depth profiles were measured by Auger electron spectroscopy (AES, PHI Model 660 Scanning Auger Microprobe, Physical Electronics) and X-ray Photoelectron Spectroscopy (XPS, PHI 5600 CI, Physical Electronics, Excitation: Mg-K $\alpha$  radiation, sputtering: Ar $^{+}$ -ions  $3.5\text{ keV}$ ,  $3\text{ nm/min}$  sputter abrasion). The structure was analysed by X-ray diffraction in Bragg–Brentano geometry (XRD, Phillips PW 3400, Co-K $\alpha$  radiation) and the texture by pole figure measurements using a Philips X'Pert 108 Texture Goniometer with

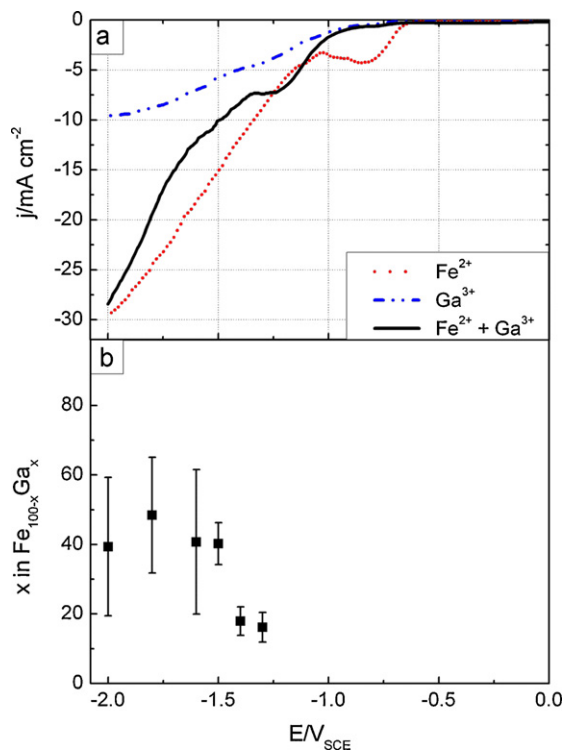


**Fig. 1.** (a) Current–potential curves of single element and complete electrolytes on Au substrates, scan rate  $10\text{ mV s}^{-1}$  and (b) ratio of Ga in potentiostatically deposited  $\text{Fe}_{100-x}\text{Ga}_x$  films on Au substrates in dependence on the deposition potential.

Cu-K $\alpha$  radiation. For magnetic measurements a vibration sample magnetometer (VSM, Quantum Design PPMS) at  $300\text{ K}$  was used. Hysteresis loops were measured parallel and perpendicular to the substrate plane using low background signal quartz holders.

## 3. Results and discussion

In order to identify the suitable potential range for the co-deposition of Fe and Ga potentiodynamic current–potential curves of both single element and complete electrolytes have been performed, shown in Fig. 1. The cathodic polarization of pure Fe solution (red dotted curve in Fig. 1a) starts with a first step at  $-0.6\text{ V}$  which is attributed to proton reduction. The following strong current increase, starting at around  $-1.05\text{ V}$ , represents the iron reduction overlapped by water decomposition. The current–potential curve of the pure  $\text{Ga}^{3+}$  solution (blue dashed curve in Fig. 1a) is characterized by a continuous current increase starting at  $-0.7\text{ V}$ . The first step observed in  $\text{Fe}^{2+}$  solution does not occur, pointing out the inhibition of proton reduction. This, as well as the much smaller slope compared to the  $\text{Fe}^{2+}$  solution, might be explained by a passivation of the electrode surface by hydrolysis products of Ga. The starting point of  $\text{Ga}^{3+}$  reduction cannot be identified because of its potential overlapping with the one for water decomposition. The behaviour of the complete electrolyte (black solid curve in Fig. 1a) is similar to the  $\text{Ga}^{3+}$  solution down to  $-0.95\text{ V}$ . Afterwards a two step behaviour is observed that approaches the current density of the iron solution at potentials around  $-2.0\text{ V}$ .

Potentiostatic deposition experiments from the single element solutions provide stable films at potentials  $E \leq -1.0\text{ V}$  for iron and  $E \leq -1.8\text{ V}$  for Ga, in contrast to the results reported by Flamini et al. [24] who quote the suitable deposition potential for Ga as  $E \leq -1.58\text{ V}$ . Potentiostatically deposited films from the complete electrolyte are unstable at potentials more positive than  $-1.3\text{ V}$ , dissolving immediately under gas evolution after stopping

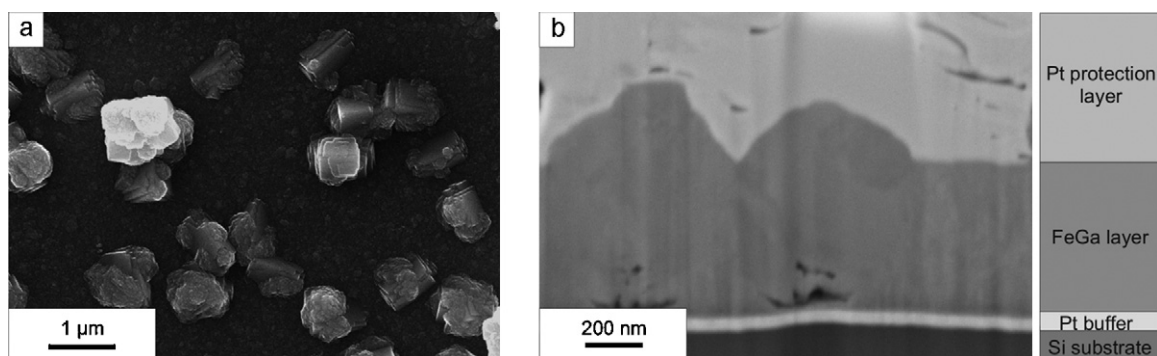


Fig. 2. SEM surface image (a) and FIB cross section (b) of a  $E_1 = -1.5$  V,  $E_2 = -0.9$  V ( $t_1 = t_2 = 10$  s) pulse-deposited  $\text{Fe}_{80}\text{Ga}_{20}$  film.

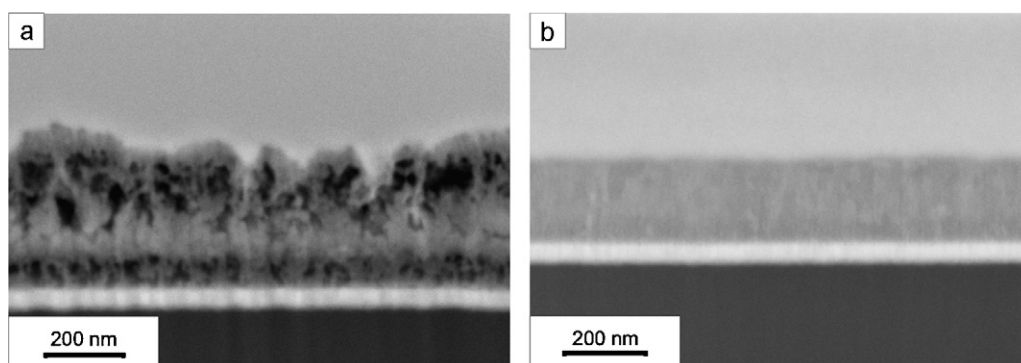


Fig. 3. FIB cross sections of pulse-deposited Fe–Ga films at different pre-conditions: (a) deposition started 1200 s after immersing electrode into electrolyte and (b) immersing electrode into electrolyte under potential applied.

the deposition. However, at  $E = -1.3$  V and lower potentials stable films are obtained. As shown in Fig. 1b the Ga ratio in  $\text{Fe}_{100-x}\text{Ga}_x$  increases to a maximum value of around 50 at.% with decreasing potential but with high uncertainty due to film inhomogeneities caused by a strong hydrogen evolution. The desired composition of about  $\text{Fe}_{80}\text{Ga}_{20}$  is obtained at  $-1.3$  V  $\leq E \leq -1.4$  V with comparatively minor changes.

For all following depositions the substrate was changed from Au to Pt. This allows later X-ray diffraction analysis of the crystalline structure of the deposited films by avoiding the overlap of substrate and film reflections. To achieve the desired composition of  $\text{Fe}_{80}\text{Ga}_{20}$  on Pt an offset of the deposition potential to  $-1.5$  V was essential. This potential offset is obviously associated with the catalytic activity of the Pt substrate, enhancing proton reduction and sub-

sequent strong interactions of the amphoteric  $\text{Ga}^{3+}$  ions and/or its hydrolysis products with the substrate surface. The detailed reduction mechanism is beyond the scope of this article and will be the subject of a further study.

Potentiostatically deposited films were hardly reproducible showing irregular morphologies and oxygen contents of up to 50 at.% as determined by SEM/EDX. Both, the inhomogeneous morphology and the high oxygen content were expected to be avoided by applying appropriate potential pulses. While keeping the deposition potential constant ( $E_1 = -1.5$  V) a second “off”-potential  $E_2 = -0.9$  V was introduced and both potentials were applied 60 times for  $t_1 = t_2 = 10$  s. SEM analysis reveals an almost smooth surface morphology with a high number of large grains growing out of the film (see Fig. 2a). FIB cross sections (Fig. 2b) show a dense

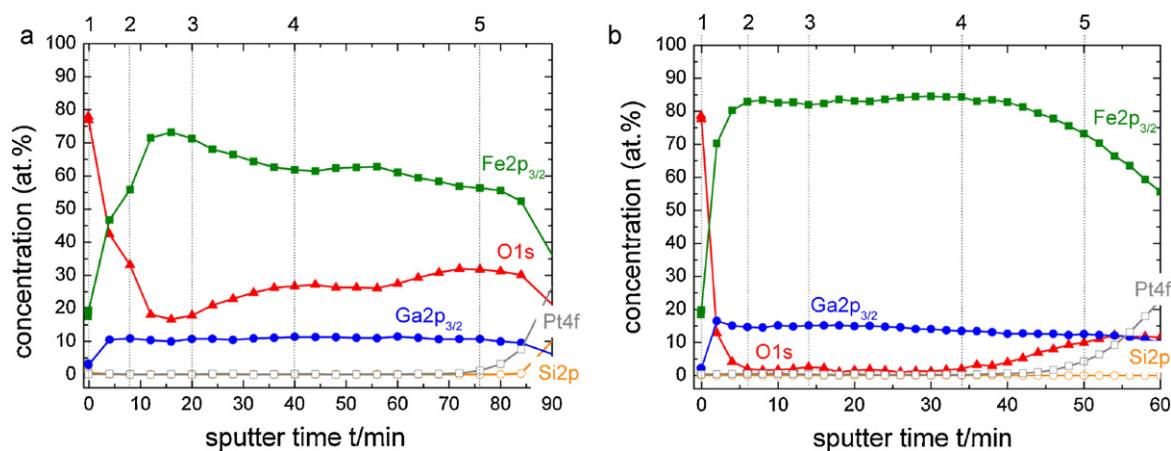
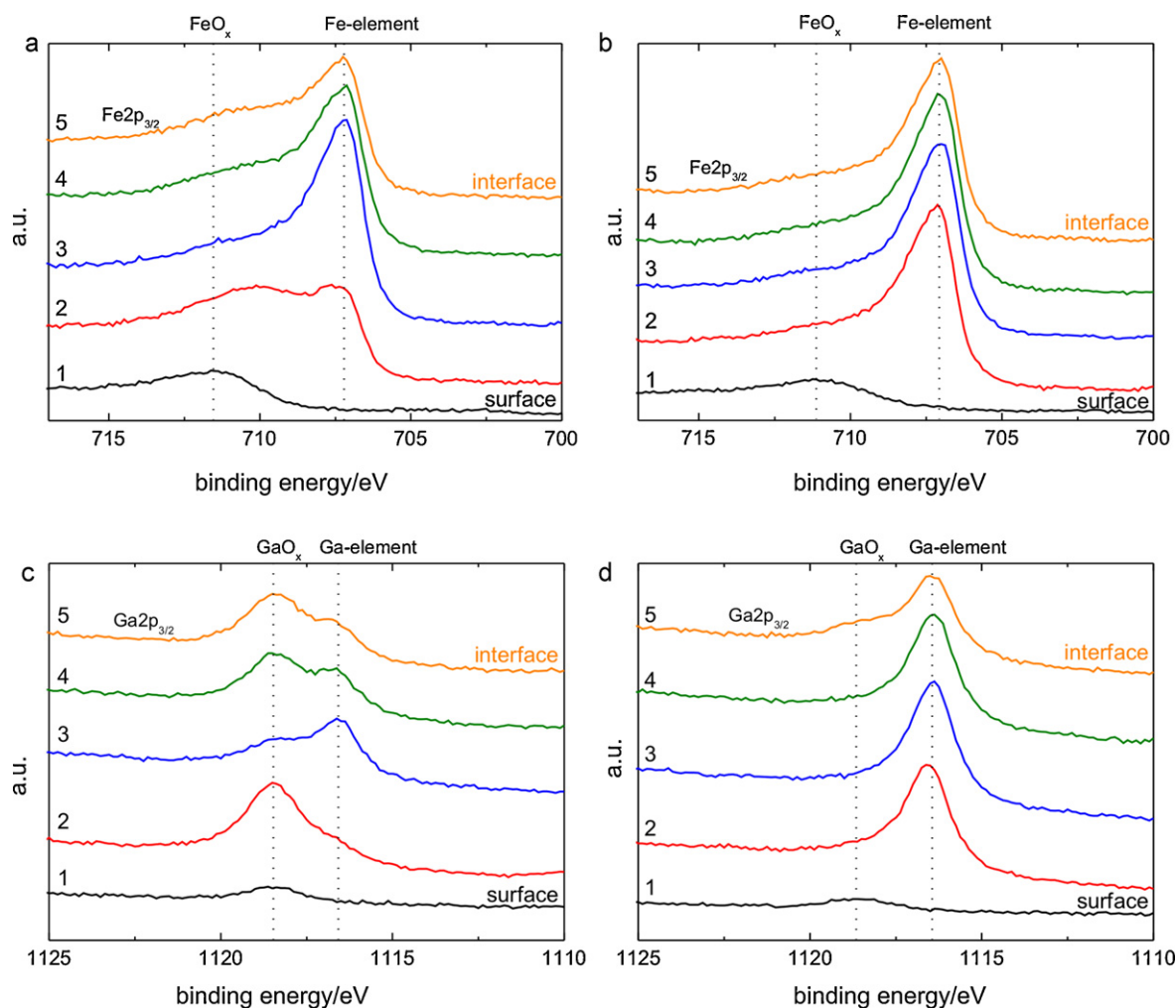


Fig. 4. XPS depth profiles of pulse-deposited Fe–Ga films at different pre-conditions: (a) deposition started 1200 s after immersing electrode into electrolyte and (b) immersing electrode into electrolyte under potential applied.



**Fig. 5.** XPS spectra of iron (a and b) and gallium (c and d) at different sputter depth (marked in Fig. 4): (a) and (c) deposition started 1200 s after immersing electrode into electrolyte and (b) and (d) immersing electrode into electrolyte under applied potential.

layer with compact particles. At the bottom of each particle pores were observed that are most probably originate from gas bubbles evolved at the initial stages of deposition.

Aiming at homogeneous, dense films without outgrowing particles these pores have to be avoided. This again requires further investigation of the initial stages of deposition. To do this two border cases have been intensively investigated: (A) the deposition potential is applied 1200 s after immersing the working electrode into the electrolyte and (B) the working electrode is immersed to the electrolyte under applied deposition potential.

Whereas the Fe/Ga atomic ratio of both films is identical at  $\sim 0.78$  the overall thickness of film (A) with  $\sim 400$  nm exceeds the thickness of film (B) with  $\sim 200$  nm by almost a factor of 2. Furthermore, FIB cross sections reveal strong differences in film morphology (Fig. 3). An inhomogeneous, porous and dendritic like growth in three different stages is observed for sample (A) (Fig. 3a). Sample (B) (Fig. 3b) is a dense and homogeneous film without any pores. Here, grain like contrasts can be seen in the FIB cross section indicating a metallic deposit.

In order to analyse the oxygen content and its distribution over film thickness in more detail AES and XPS depth profiles have been measured. The related XPS profiles starting from the film surface down to the film–substrate interface of samples (A) and (B) are compared in Fig. 4a and b, respectively. Similar results were obtained by AES depth profiles measurements and therefore are not shown here. For both samples the Fe:Ga atomic ratio can be esti-

mated as 85:15 in reasonable agreement with the EDX data given above. The deviation of  $\sim 7$  at.% might be related to the sum of the systematic errors (use of standard sensitivity factors, preferential sputtering) of both methods. The increase of the Pt and later the Si signal indicates that the substrate surface is reached.

In general, the XPS profiles show a high oxygen content of 20–30 at.% for sample (A) and a much lower oxygen content of 1–10 at.% for sample (B). Directly at the sample surface both samples show a high oxygen content up to 80 at.% indicating a strong affinity to surface oxidation. Afterwards both samples strongly differ from each other. The oxygen content in sample (A) only slowly reduces to a relatively high minimum value of 20 at.%. The most probable reason for this slow decrease is the high porosity and therefore high surface-to-volume ratio observed in the cross section (Fig. 3a). With increasing sputter depth the oxygen content again increases up to 30 at.%. In the lower third of the film thickness the oxygen content again slightly decreases to a final value of around 28 at.%. Due to the high porosity of the film oxygen surface diffusion might be strongly enhanced therefore influencing the accuracy of the results.

Contrary, the oxygen content in sample (B) sharply decreases to less than 1 at.% within the first 20 nm (4–6 min sputter depth). This value remains constant over 2/3 of the film thickness and slightly increases to 11 at.% near the film–substrate interface.

Detailed information about the oxygen binding behaviour was extracted from single spectra recorded during the XPS depth profile

measurements. For both, iron and gallium characteristic selected spectra over the thickness of the films are shown in Fig. 5. The selected depth steps for both samples are marked in Fig. 4 with numbers from 1 to 5. As expected from the very high oxygen content both iron and gallium are oxidized at the sample surfaces. No metallic Fe and Ga had been determined in spectrum 1 for both samples.

For the porous and inhomogeneous sample (A) the oxygen content decreases only slowly (see Fig. 4a) and therefore oxidized species still appear in spectra 2 of Fig. 5a and c. Unlike Ga that is still completely oxidized metallic Fe already arises. The Fe spectra 3–5 (Fig. 5a) show mostly metallic Fe and only a minor fraction of oxidized Fe species. Spectrum 3 of Ga (Fig. 5c) shows mainly metallic gallium with a minor portion of oxidized Ga whereas this trend is again reversed in spectra 4 and 5 with more oxidized than metallic Ga.

In contrast to these results the spectra 2–5 of the dense and homogeneous sample (B) show nearly pure metallic peaks for both iron (Fig. 5b) and gallium (Fig. 5d) over the whole film thickness. No trace of oxidized species is observed in spectra 2–4 in agreement with the low oxygen content of only about 1 at.% found in this region. Spectrum 5 of gallium near the interface to the substrate (Fig. 5d) reveals a slight decrease of the metallic quantity and a marginal shoulder of oxidized Ga shows up.

Even though the particular deposition mechanism is not known in detail, the combination of the obtained results gives important hints for the process occurring: strong interactions of the electrolyte components, mainly  $\text{Ga}^{3+}$  ions or its hydrolysis products, with the Pt substrate lead to the formation of a passivating film at the interface between electrolyte and substrate. Once a passivating film is formed electrodeposition can occur only at defects in this film or at high overpotentials favoring dendritic growth as well as hydrogen evolution and the formation of highly porous films with high surface area. After terminating the deposition the high surface area immediately tends to form a surface oxide layer. On the other hand, if the deposition is immediately started once the electrolyte comes into contact with the substrate, these interactions are almost completely prevented. Thereby avoiding strong passivation can prevent both dendritic growth and high oxygen content. As a result dense films with oxygen contents as low as 1 at.% can be obtained that are required for magnetostrictive applications.

The XRD pattern of the homogeneous, dense sample is presented in Fig. 6a. Besides the substrate reflection of Si( $82^\circ$ ) and Pt( $46^\circ$ ,  $104^\circ$ ) only one intense reflection at  $52.1^\circ$  occurs that can be assigned to the (1 1 0) reflection of the thermodynamically stable  $\alpha\text{-Fe}_3\text{Ga}$  phase exhibiting a disordered bcc structure. A very weak reflection related to (2 1 1)  $\text{Fe}_3\text{Ga}$  is additionally observed at  $98.4^\circ$ . As the (1 0 0) and (2 0 0) reflections of  $\text{Fe}_3\text{Ga}$  are absent these results indicate a strongly preferred (1 1 0) orientation. Additional texture measurements of the (1 1 0) pole figure (see Fig. 6b) show an intense central spot at  $\psi < 10^\circ$  and a ring at  $\psi = 60^\circ$ . The angle between the different {1 1 0} planes in the cubic system is  $60^\circ$ . Therefore the ring at  $60^\circ$  with equally distributed intensities combined with the central spot proves a (1 1 0) fibre texture with no preferred in plane orientation. Additionally measured (2 0 0) and (2 1 1) poles confirm the (1 1 0) fibre texture (not shown).

Magnetic properties have been obtained by measuring hysteresis loops parallel and perpendicular to the film plane and are shown for the dense film with low oxygen content in Fig. 7. The film shows a low coercivity of 4 mT parallel and 30 mT perpendicular to the substrate indicating soft magnetic behaviour. A high saturation magnetization of about 1.7 T is achieved that exceeds values reported for sputtered films of 1.45 T [21] and approaches the values for bulk single crystals of 1.75 T [2]. As expected due to shape anisotropy the easy axis of magnetization is strongly aligned within the film plane and a field close to spontaneous polarisation

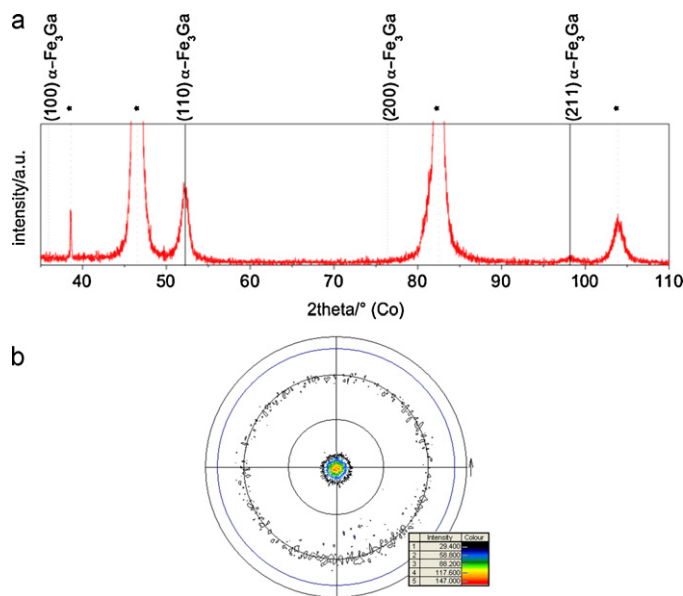


Fig. 6. XRD pattern (a) and (1 1 0) pole figure (b) of a dense, homogeneous film. Substrate reflections in the XRD pattern are marked with (\*).

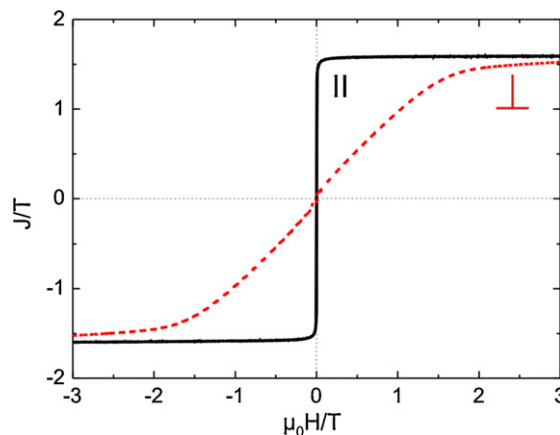


Fig. 7. Hysteresis loops of a dense layer with low oxygen content measured parallel (||) and perpendicular ( $\perp$ ) to the substrate.

is required to saturate the field out of plane. Close to saturation in both directions a noticeable curve bending is observed. This indicates the presence of some additional anisotropy, which may either originate from magnetocrystalline anisotropy or, more likely, on magnetostrictive anisotropy induced by film stress.

The magnetic measurements particularly confirm the high quality of the electrodeposited films containing only a negligible number of defects and impurity phases.

#### 4. Conclusion

FeGa alloy films with a desired composition close to  $\text{Fe}_{80}\text{Ga}_{20}$  and a (1 1 0)  $\text{Fe}_3\text{Ga}$  fibre texture have been fabricated electrochemically. Strong interactions of the electrolyte with the substrate surface are identified to cause low reproducibility and high oxygen content. Using optimized pre-treatment and pulsed potential conditions the films are dense and homogeneous. The oxygen content was reduced to less than 1 at.% and the saturation magnetization reaches up to 1.7 T, confirming the high quality of these films. These results show that electrodeposition can be most effectively used to grow  $\text{Fe}_{80}\text{Ga}_{20}$  films for application in magnetostrictive actuating and sensing devices

## Acknowledgement

The authors thank K. Hennig for FIB investigations.

## References

- [1] B.D. Cullity, C.D. Graham, *Introduction to Magnetic Materials*, John Wiley and Sons Inc., NJ, 2009.
- [2] A.E. Clark, M. Wun-Fogle, J.B. Restorff, K.W. Dennis, T.A. Lograsso, R.W. McCallum, *J. Appl. Phys.* 97 (2005) 10M316.
- [3] E.M. Summers, T.A. Lograsso, M. Wun-Fogle, *J. Mater. Sci.* 42 (2007) 9582–9594.
- [4] A. Javed, N.A. Morley, M.R.J. Gibbs, *J. Magn. Magn. Mater.* 321 (2009) 2877–2882.
- [5] C. Mudivarthi, M. Laver, J. Cullen, A.B. Flatau, M. Wuttig, *J. Appl. Phys.* 107 (9) (2010) A957.
- [6] R.C. Hall, *J. Appl. Phys.* 30 (1959) 816–819.
- [7] R.C. Hall, *J. Appl. Phys.* 31 (1960) 1037–1038.
- [8] A.E. Clark, J.B. Restorff, M. Wun-Fogle, T.A. Lograsso, D.L. Schlager, *IEEE Trans. Magn.* 36 (2000) 3238–3240.
- [9] R.R. Basantkumar, B.J.H. Stadler, W.P. Robbins, E.M. Summers, *IEEE Trans. Magn.* 42 (2006) 3102–3104.
- [10] P.D. McGary, L.W. Tan, J. Zou, B.J.H. Stadler, P.R. Downey, A.B. Flatau, *J. Appl. Phys.* 99 (2006) 308–310.
- [11] H.M. Schurter, Y. Zhang, R. Wu, A.B. Flatau, *Proc. SPIE* 7289 (2009) 72891Y.
- [12] C. Wenzel, B. Adolphi, U. Merkel, A. Jahn, U. Marschner, J. Ziske, H. Neubert, W.-J. Fischer, *Sens. Actuators A* 156 (2009) 129–133.
- [13] P.R. Downey, A.B. Flatau, P.D. McGary, B.J.H. Stadler, *Proc. SPIE* 6932 (2008) 69320P.
- [14] S. Armyanov, *Electrochim. Acta* 45 (2000) 3323–3335.
- [15] T.A. Lograsso, A.R. Ross, D.L. Schlager, A.E. Clark, M. Wun-Fogle, *J. Alloys Compd.* 305 (2003) 95–101.
- [16] J.R. Cullen, A.E. Clark, M. Wun-Fogle, J.B. Restorff, T.A. Lograsso, *J. Magn. Magn. Mater.* 226 (2001) 948–949.
- [17] R.A. Kellogg, A.M. Russell, T.A. Lograsso, A.B. Flatau, A.E. Clark, M. Wun-Fogle, *Acta Mater.* 52 (2004) 5043–5050.
- [18] A. Butera, J. Gómez, J.A. Barnard, J.L. Weston, *Physica B* 384 (2006) 262–264.
- [19] R.A. Dunlap, J.D. McGraw, S.P. Farrell, *J. Magn. Magn. Mater.* 305 (2006) 315–320.
- [20] B.W. Wang, S.Y. Li, Y. Zhou, W.M. Huang, S.Y. Cao, *J. Magn. Magn. Mater.* 320 (2008) 769–773.
- [21] B. Adolphi, J. McCord, M. Bertram, C.-G. Oertel, U. Merkel, U. Marschner, R. Schäfer, C. Wenzel, W.-J. Fischer, *Smart Mater. Struct.* 19 (2010) 055013.
- [22] E. Reichel, *Fresenius J. Anal. Chem.* 87 (1932) 321–332.
- [23] W.M. Saltman, N.H. Nachtrieb, *J. Electrochem. Soc.* 100 (1953) 126–130.
- [24] D.O. Flaminio, S.B. Saidman, J.B. Bessone, *J. Appl. Electrochem.* 37 (2007) 467–471.
- [25] A. Brenner, *Electrodeposition of Alloys*, Academic Press Inc., NY, 1963.
- [26] P.D. McGary, B.J.H. Stadler, *J. Appl. Phys.* 97 (2005) 10R503.
- [27] N. Lupu, H. Chiriac, P. Pascariu, *J. Appl. Phys.* 103 (07) (2008) B511.
- [28] N. Lupu, P. Pascariu, C. Gherasim, H. Chiriac, *IEEE Trans. Magn.* 44 (2008) 3005–3008.
- [29] P.D. McGary, K.S.M. Reddy, G.D. Haugstad, B.J.H. Stadler, *J. Electrochem. Soc.* 157 (2010) D656–D665.